Check for updates

Wiley
Journal of Sensors
Volume 2026, Article ID 8045999, 12 pages
https://doi.org/10.1155/js/8045999

WILEY

Research Article

Wideband Single-Layer Reflectarray Antenna for Millimeter-Wave 5G Communications

S. D. Khan,[1] **M. I. Abbasi**,[1] **I. M. Ibrahim**,[1] **N. H. Sulaiman**,[2] **M. H. Dahri**,[3] **M. A. Humayun**,[4] **and Hela Elmannai**[5]

[1]*Faculty of Electronic and Computer Engineering and Technology (FTKEK), Universiti Teknikal Malaysia Melaka, Durian Tunggal, Malacca 76100, Malaysia*
[2]*Faculty of Engineering Technology, Universiti Tun Hussein Onn Malaysia, Pagoh Higher Education Hub 84600, Pagoh, Muar, Johor, Malaysia*
[3]*Department of Telecommunication Engineering, Dawood University of Engineering and Technology, Karachi 74800, Sindh, Pakistan*
[4]*Department of Electrical and Electronic Engineering, Faculty of Engineering and Technology, Eastern University, Dhaka 1345, Bangladesh*
[5]*Department of Information Technology, College of Computer and Information Sciences, Princess Nourah Bint Abdulrahman University, P.O. Box 84428, Riyadh 11671, Saudi Arabia*

Correspondence should be addressed to M. I. Abbasi; inamabbasi@utem.edu.my and M. A. Humayun; humayun.eee@easternuni.edu.bd

Received 5 May 2025; Revised 14 October 2025; Accepted 19 November 2025

Guest Editor: Deepali

Copyright © 2026 S. D. Khan et al. Journal of Sensors published by John Wiley & Sons Ltd. This is an open access article under the terms of the Creative Commons Attribution License, which permits use, distribution and reproduction in any medium, provided the original work is properly cited.

The rapid evolution of intelligent applications has driven the demand for high-performance antenna systems. Reflectarrays (RAs), also referred to as planar reflectors, have emerged as a promising solution for modern wireless and satellite communication systems due to their beam-steering capability and high-gain characteristics. This study presents a comprehensive analysis of a novel unit cell geometry and its simulated design for RA antennas operating in the millimeter-wave (mm-wave) band at 28 GHz, aiming to enhance performance metrics such as bandwidth, phase agility, and efficiency for its applications in 5G communication systems. The proposed unit cell consists of a rectangular patch with a set of strategically embedded slot configurations in order to achieve optimum performance based on surface current modification. For the periodic array, initially, a 21×21 element array was designed and then the corner elements were truncated to form a 357 elements array in circular configuration. The proposed RA demonstrated a gain of 21.4 dB, for a tilted beam formed at 19° using a center feed horn. More importantly, the proposed RA achieved a significantly improved 1-dB gain bandwidth of over 23.21% for a frequency range of 26.5-GHz which can be used in mm-wave applications such as 5G communication systems.

Keywords: broadband; high gain; millimeter-wave reflectarray; slot embedded patch

1. Introduction

A reflectarray (RA) antenna is an advanced hybrid antenna system that integrates the benefits of both conventional reflector and array antennas. It comprises a planar surface with a meticulously engineered arrangement of radiating elements that manipulate the phase of reflected electromagnetic waves [1]. The phase shift of each unit cell is precisely controlled through parameters such as geometry, size, orientation, and material composition, enabling tailored wavefront shaping. By optimizing the phase distribution across the surface, RAs achieve high gain, low profile, and dynamic beam-steering capabilities, making them highly suitable for next-generation wireless and satellite communications [2, 3].

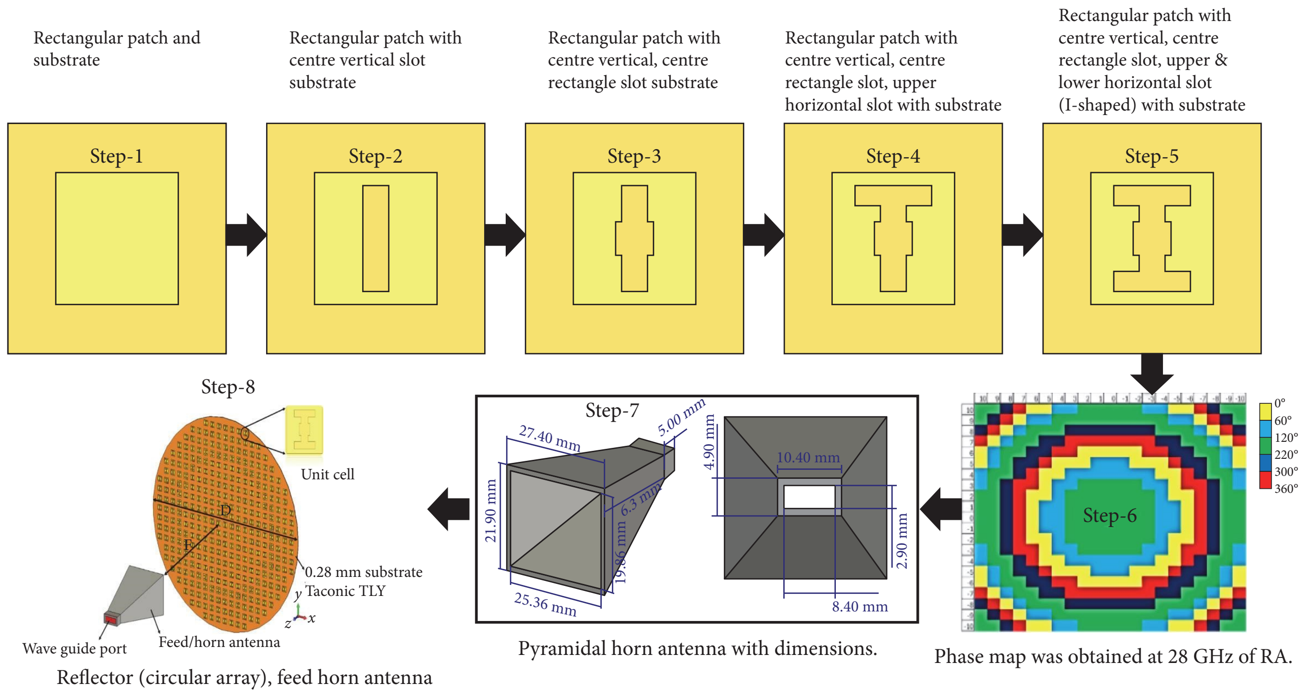

FIGURE 1: Stages of evolution of the proposed I-shaped RA unit cell and RA designing.

In the millimeter-wave (mm-wave) spectrum, ongoing research focuses on enhancing the beam-steering performance of these antennas to improve directivity, signal strength, and overall system efficiency. Various beam-steering methodologies, including electronic, mechanical, and tunable meta surface-based approaches, have been explored, each offering distinct trade-offs in terms of complexity, power consumption, and implementation feasibility [4–6]. Beam-steering refers to the capability of dynamically adjusting an antenna's radiation pattern to optimize signal transmission and reception in a specific direction, typically achieved through precise phase modulation of the reflected wave [7, 8].

Both RAs and transmitarrays (TAs) are extensively utilized in the development of high-gain antennas, each presenting unique advantages based on system requirements. The adaptability and precision of RA-based beamforming make them an attractive solution for 5G, satellite communications, radar systems, and next-generation wireless networks, where real-time control over radiation characteristics is critical for achieving optimal performance.

Berry initially proposed the idea of the RA antenna in 1963 [9], but until additional research showed its viability and wide range of applications in the 1990s, its employability was mainly unrealized [1]. Since then, RA antennas have been thoroughly studied in a number of frequency bands for use in wireless power transmission, imaging, radar systems, and satellite communications [10–15]. Although, electrically reconfigurable RA antennas have made great strides, they are still usually limited to a single operating mode [16–19] and frequently have performance issues because of the incorporation of active electronic components [20–22].

However, because of the radiation elements' constrained bandwidth, RAs are inherently restricted. Furthermore, some broadband features—such as fractured elements [23] and fractal elements [24], face difficulties in the mm-wave spectrum because of manufacturing tolerances.

Using well-known design techniques, like multilayer multiresonance elements [25, 26], true-time delay elements [27, 28], sub-wavelength elements [29], single-layer elements, and newly developed 3D-printed dielectric resonators and metal-only elements, respectively, several studies suggest novel RA elements to achieve broadband and high-gain performance for mm-wave applications. Multilayer RA are one of the possible options for the design of broadband RAs, however, is a difficult procedure that demands greater accuracy and raises costs [30]. In this work, a broadband RA has been proposed, where the unit cell comprises of a rectangular patch element with multiple embedded slots placed technically to modify the surface current distribution. Furthermore, a periodic array of 357 strategically placed elements has also been designed based on the required progressive phase distribution and its performance is analyzed for the proposed mm-wave applications.

2. Design of the Proposed Unit Cell

In this work, of designing unit cell for RA antennas, an infinite RA with a 0.035 mm patch element thickness (copper) and Taconic TLY 3FF substrate with 0.28 mm thickness was created using a commercially available CST MW computer model. The patch elements and ground plane were designed using copper with a conductivity of 59.6 Ms/m at 20°C.

An inventive method for creating a planar RA unit cell with a smoothly fluctuating phase distribution is presented in this research. As seen in Figure 1, the suggested design includes an I-shaped unit cell that resonantly operates at 28 GHz and incorporates slots that are positioned strategically across the patch. For mm-wave applications, these slots are essential for effectively converting spherical waves into planar waves, which

9161, 2026, 1, Downloaded from https://onlinelibrary.wiley.com/doi/10.1155/js/8045999 by Muhammad Inam Abbasi - National Institutes Of Health Malaysia , Wiley Online Library on [11/01/2026]. See the Terms and Conditions (https://onlinelibrary.wiley.com/terms-and-conditions) on Wiley Online Library for rules of use; OA articles are governed by the applicable Creative Commons License

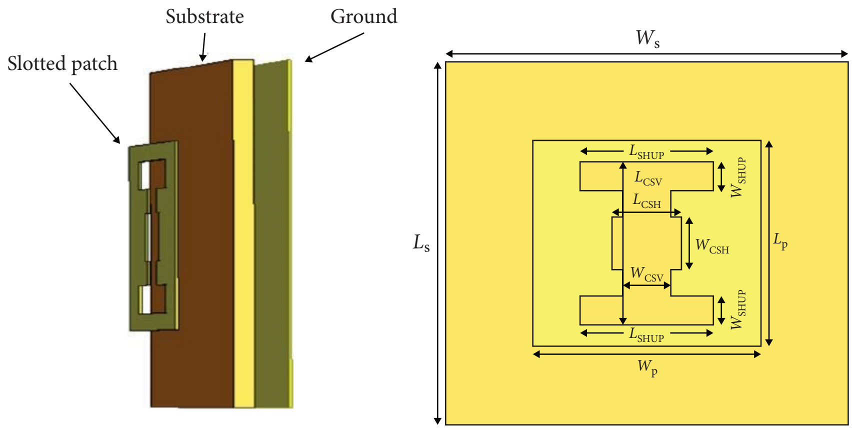

FIGURE 2: Unit cell of a planar reflector with dimensions and 3D view.

improves the reflector's performance and efficiency. Figure 1, delineates a comprehensive design and analysis framework for a RA antenna, showcasing the progressive development of the unit cell geometry and its incorporation into the full system architecture.

Steps 1–5: The iterative refinement of the unit cell structure is depicted, beginning with a basic rectangular patch and sequentially incorporating slots and structural modifications to optimize phase response and enhance bandwidth performance.

Step 6: The simulated phase distribution across the RA surface is presented, illustrating the engineered phase gradient necessary for effective beamforming and aperture efficiency.

Step 7: The configuration of the horn antenna is detailed, including its geometric parameters and spatial orientation relative to the RA, ensuring optimal feed illumination and minimal spillover losses.

Step 8: Final system integration: the fully assembled RA antenna is shown, comprising an array of meticulously designed unit cells tailored to achieve precise beamforming characteristics at the target operating frequency.

This methodical approach is essential for maximizing the electromagnetic performance of the RA, enabling high gain, accurate beam steering, and reduced phase errors at the designated operational frequency.

Figure 2, presents the details of the design with labels for each of the dimensions. Initially the unit cell was designed and optimized for 28 GHz resonance frequency as shown in Figure 3a. For the initial design, the numerical values of the dimensions are provided in Table 1. It can also be observed from Table 1, that all the three slots employed to obtain the desired configurations are dependent on the length and width of the patch. This technique provides a trivial method for the optimization of the unit cell and obtaining its progressive phase distribution. Moreover, for the RA design one of the important steps is to sweep the resonance throughout the desired frequency range. This has also been achieved by simply varying the length of the patch and keeping into account that the length of all the slots will be varied as they are dependent on patch length. Figure 3b,c shows the effect of varying the patch length on the reflection loss and reflection phase. It can be observed by the demonstrated results, that by varying the patch length from 2.41 to 3.41 mm, the reflection loss varies only from 0.35 to 0.45 dB for the whole sweep while the resonance is varied in a wide frequency range from 22 to 34 GHz frequency range.

Figure 3d presents the progressive phase and loss plotted against the length of patch at a resonant frequency of 28 GHz. It can be observed from the results that for the proposed design configuration, the reflection loss is only −0.38 dB while the reflection phase plot covers a phase range close to 343°. Ideally, the phase coverage should be 360°, but practically this cannot be achieved, and 17° phase errors are considered adequate for RA design. Furthermore, for the characterization of the proposed unit cell, bandwidths have been calculated at 10% and 20% of maximum loss. The 10% and 20% bandwidth are observed to be 1.2 and 1.7 GHz respectively while the slope of reflection phase curve is observed to be 5.67°/MHz. This progressive phase distribution shows satisfactory values for the periodic array design and is used in this work for complete RA design.

3. Proposed RA Antenna Design

The RA antenna is basically analogous to a parabolic reflector antenna, however, unlike the parabola, the reflection phase adjustment towards a focus point in a RA is done by the phase calculation of each of the unit cells. Apart from a planar reflector design, RA needs a suitable source, usually a horn antenna, that can provide the desired performance. This section covers the basic elements of RA design, that are, mathematical calculations of desired phase, design of horn antenna, as well as the periodic reflector design.

3.1. Element Phase Distribution in an Array. The phase distribution on the RA aperture is fundamentally pixelated which is essentially the progressive phase to the aperture, and is given by,

$$\varphi_n = R_i = \sqrt{\left(\left(\left(x_i - x_f\right) + \left(y_i - y_f\right) + z_f\right)\right)}. \quad (1)$$

The Equation (1) is vital in the design of RA antennas, with φ_n is a phase constant, indicating that a relative phase is

9161, 2026, 1, Downloaded from https://onlinelibrary.wiley.com/doi/10.1155/js/8045999 by Muhammad Inam Abbasi - National Institutes Of Health Malaysia , Wiley Online Library on [11/01/2026]. See the Terms and Conditions (https://onlinelibrary.wiley.com/terms-and-conditions) on Wiley Online Library for rules of use; OA articles are governed by the applicable Creative Commons License

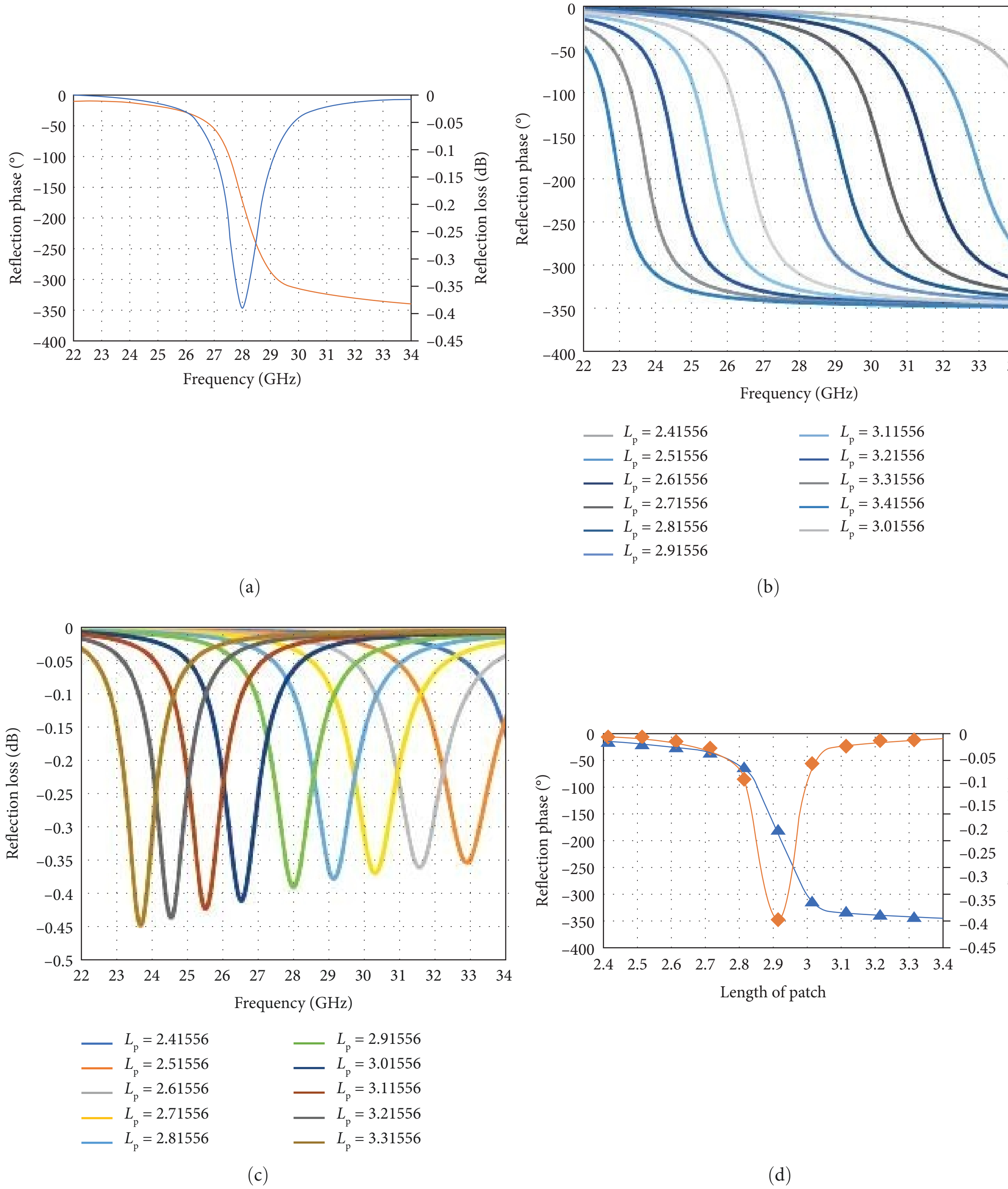

Figure 3: (a) Reflection loss and reflection phase at 28 GHz, (b) progressive reflection phase, (c) progressive reflection loss (dB), and (d) progressive reflection phase vs. length of patch.

needed for the RA elements. In RA design, each unit cell is positioned at an individual coordinate $(x_i, x_f, 0)$ on the array surface, which indicates the distance from the feed source located at (x_i, x_f, z_f) to the i^{th} unit cell. The distance influences the phase delay encountered by the wave as it travels from the feed source to the unit cell. To achieve a coherent reflected wavefront in the intended direction, the phase shift introduced by each unit cell must be modified to account for the path difference R_i. Systematic calculation of R_i for all unit cells allows for the application of the essential phase correction to align reflected waves, thereby facilitating efficient beamforming and improving antenna gain. This equation is crucial

9161, 2026, 1, Downloaded from https://onlinelibrary.wiley.com/doi/10.1155/js/8045999 by Muhammad Inam Abbasi - National Institutes Of Health Malaysia , Wiley Online Library on [11/01/2026]. See the Terms and Conditions (https://onlinelibrary.wiley.com/terms-and-conditions) on Wiley Online Library for rules of use; OA articles are governed by the applicable Creative Commons License

Table 1: Dimension of frequency switchable I-shaped unit cell of reflectarray antenna.

Substrate (mm)		Patch (mm)		Slot horizontal upper and lower (mm)		Center slot horizontal (mm)		Center slot vertical (mm)	
Length	Width	Length	Width	Length	Width	Length	Width	Length	Width
L_s	W_s	L_p	W_p	L_{SHUP}	W_{SHUP}	L_{CSH}	W_{CSH}	L_{CSV}	W_{CSV}
Lambda/2	Lambda/2	L_p	W_p	$L_p/2\times0.60$	$W_p/2\times0.30$	$L_p/2\times0.30$	$W_p\times0.25$	$W_p\times0.1$	$L_p\times0.386$
5.35	5.35	3.13	3.01	0.45	2.24	0.75	0.94	0.60	2.44

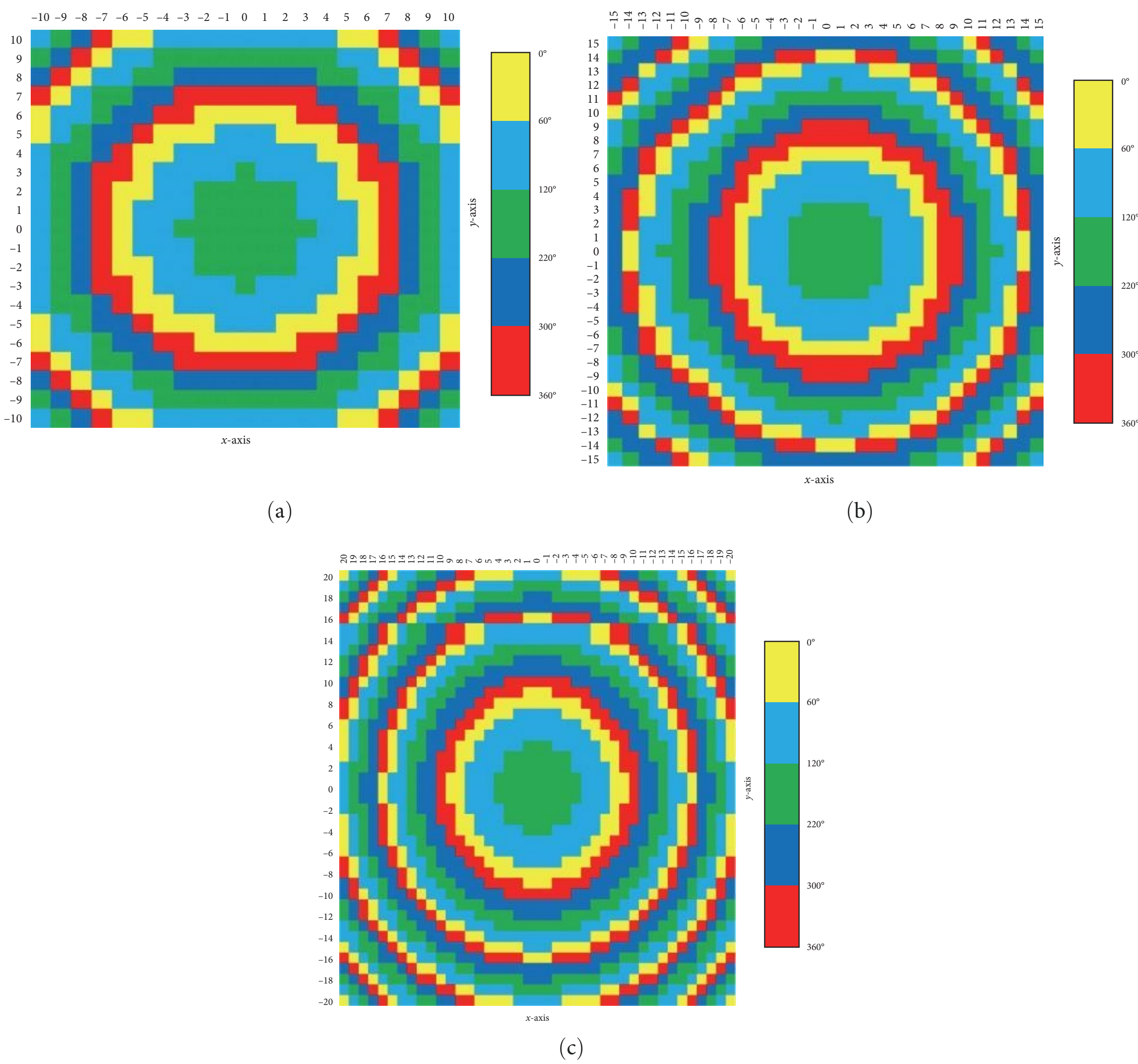

Figure 4: The phase map was obtained at 28 GHz of RA. (a) 21×21 elements, (b) 31×31 elements, and (c) 41×41 elements.

for adjusting the phase response of unit cells and enhancing the overall performance of the RA. The phase map of 21×21 (10λ), 31×31 (15λ) and 41×41 (20λ) is calculated by using Equation (1), shown in Figure 4a–c, respectively. It can be observed form Figure 4 that as the number of elements in the arrays is increased, the phase distribution becomes more focused which will provide better results in terms of gain as expected. However, increasing the size of array will add up the cost in terms of simulation resources as well as fabrication using high quality materials. Therefore, in this work 21×21 element array has been used using the required phase distribution achieved by Equation (1).

3.2. Feed/Horn Antenna Design. The design and performance of RA antennas depend critically on the feed horn antenna especially in mm-wave applications. The feed horn's design must also consider the limited beamwidth and high directed gain needed at mm-wave frequencies, where system losses

9161, 2026, 1, Downloaded from https://onlinelibrary.wiley.com/doi/10.1155/js/8045999 by Muhammad Inam Abbasi - National Institutes Of Health Malaysia , Wiley Online Library on [11/01/2026]. See the Terms and Conditions (https://onlinelibrary.wiley.com/terms-and-conditions) on Wiley Online Library for rules of use; OA articles are governed by the applicable Creative Commons License

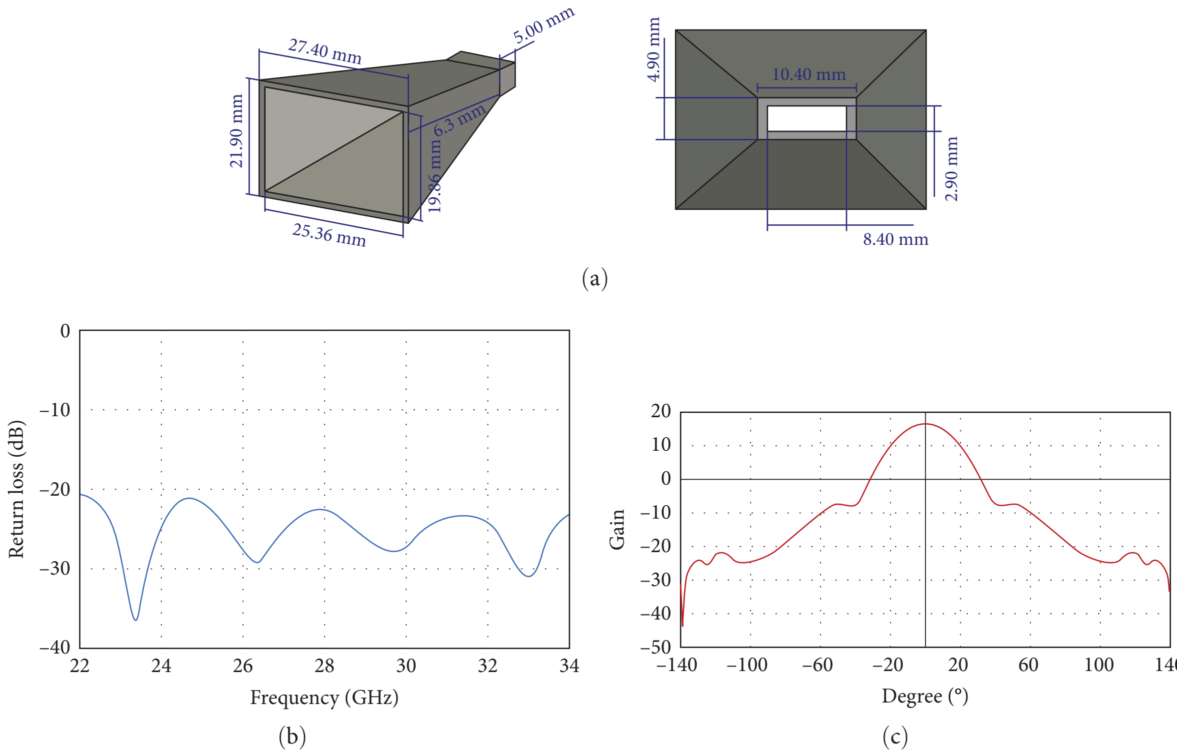

Figure 5: Pyramidal horn antenna (a) Perspective and back view with dimensions, (b) Return loss, and (c) far-field 1-D Cartesian plot at 28 GHz.

and ambient attenuation can dramatically affect performance. Thus, maximizing the general efficiency and functionality of the mm-wave RA antenna system depends on careful evaluation of the design of the feed horn including its geometry, size, and connection with the RA elements. In this work, a standard pyramidal horn antenna has been used and simulated using CST MWS to operate within the desired frequency range of 22–34 GHz.

Figure 5a shows the design with labeled dimensions of the proposed horn antenna for the RA while Figure 5b,c provides the return loss and radiation pattern of the design horn, respectively. It can be observed from the results that throughout the desired frequency range, the return loss constantly stays below −20 dB level which is good enough for this design. Moreover, the horn antenna provides a peak gain of 18.38 dB at the desired frequency of 28 GHz. These results satisfy the requirements of the proposed RA antenna design and hence this horn antenna can be used as the feed.

3.3. Periodic RA Antenna Design 21 × 21 Elements. In order to construct a periodic RA antenna, 21 × 21 resonant element array was designed on 0.28 mm thick Taconic TLY 3FF dielectric substrate using the required phase distribution as explained above. The interelement spacing was optimized to be kept constant at 0.5 λ, as in the case of unit cells, which made the total size of the array to be 10 λ × 10 λ (118 mm × 118 mm). The proposed horn antenna is used as a center feed and was placed above the RA at a distance equal to the maximum RA dimension ($f/D = 1$). In order to avoid the complexities involved with off-set feed horn, the designed RA was tilted to an angle of $\theta_T = 10^\circ$ in the *XZ* plane as shown in Figure 6. The tilting of the RA facilitated to focus the main beam ideally at 20° away from the center avoiding any chances of potential feed horn blockage of the reflected wave. Figure 6 shows the complete topology of the proposed RA antenna.

4. Optimization of the Proposed Design

By using f/D ratios of 0.9 and 1.1 in this work of RA antenna in design provides basis for performance optimization. Usually with an f/D ratio of 0.9, a bigger beam is generated which can be helpful in applications requiring wider coverage but may also have considerably reduced gain and probable phase alignment problems. On the other hand, an f/D ratio of 1.1 favors a smaller beam and higher directivity, hence boosting gain and tightening energy focus.

Figures 7 and 8show the electromagnetic analysis carried out for the proposed RA antenna using CST MWS. It can be observed from the Figures 7a and 8a that the surface currents demonstrate maximum value at an off-set of 20° as set up earlier by tilting the array to 10°, which validates the applied concept. It can also be observed that the surface currents are more focused in the case of f/D ration of 0.9 as compared to f/D ratio of 1.1. This observation is also evident from the 2D and 3D radiation pattern curves shown in Figures 7c,d and 8c,d, respectively, where the reflected beam is more focused for 0.9 f/D, presenting a better radiation pattern and higher gain.

Figures 7b and 8b present the near field radiation of the proposed antenna. It can be observed from the results that that the beam generated by the feed horn antenna produces a

9161, 2026, 1, Downloaded from https://onlinelibrary.wiley.com/doi/10.1155/js/8045999 by Muhammad Inam Abbasi - National Institutes Of Health Malaysia , Wiley Online Library on [11/01/2026]. See the Terms and Conditions (https://onlinelibrary.wiley.com/terms-and-conditions) on Wiley Online Library for rules of use; OA articles are governed by the applicable Creative Commons License

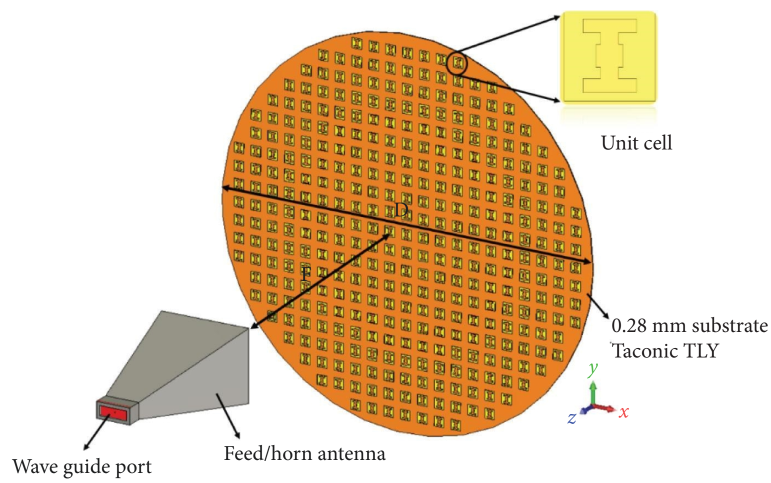

FIGURE 6: Circular reflectarray antenna with I-shaped unit cells, labeled, feed (f), focal distance (D), and a zoomed view of the unit cell.

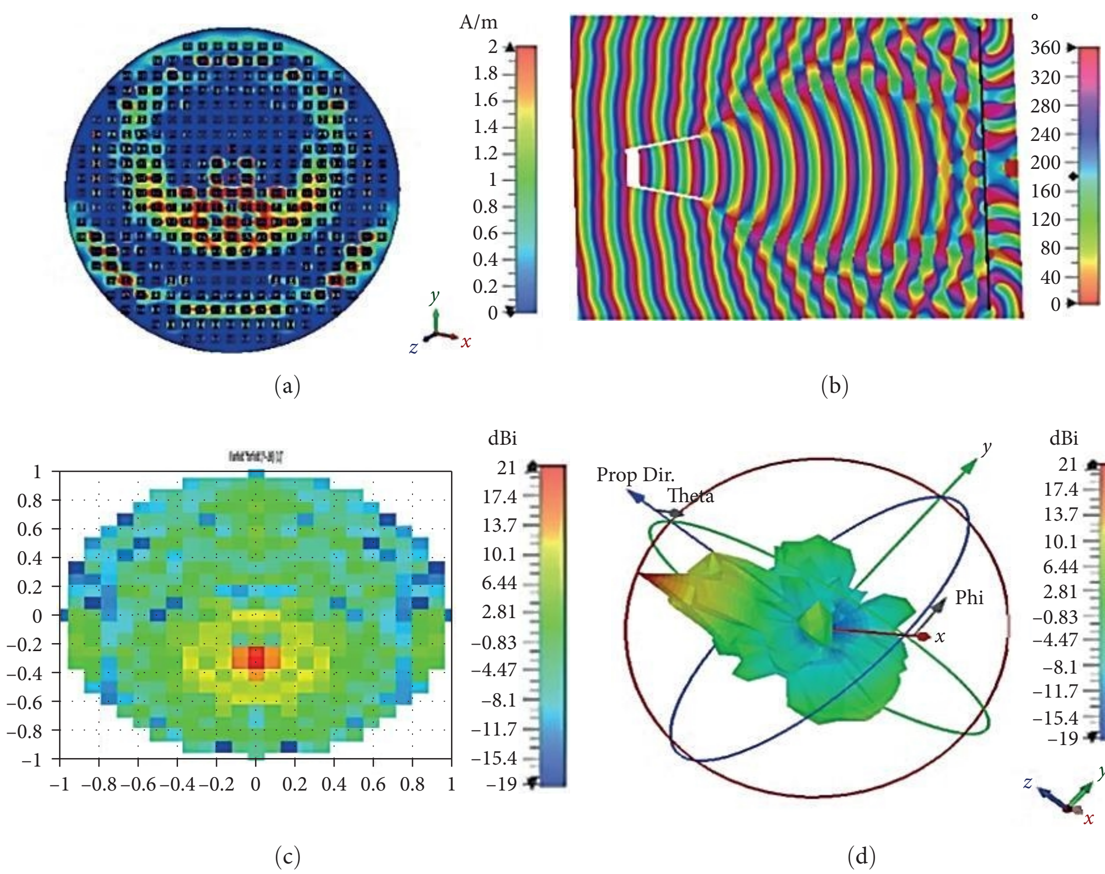

FIGURE 7: Electromagnetic analysis of a reflectarray antenna operating at 28 GHz with an f/D ratio of 0.9 (a) surface current distribution, (b) near-field phase distribution pattern, (c) 2D far-field radiation pattern, and (d) 3D far-field radiation pattern.

spherical beam which is converted into a planar wave front beyond the horn after reflection from the planar reflector. This phenomenon also validates the theoretical understanding of the RA antenna which is required to produce a planar wave in the far-field region.

Figure 9, depicts the far-field radiation of RA antenna obtained at 28 GHz for different f/D ratios in order to further optimize the radiated beam characteristics. It can be observed form Figure 9 that, for an f/D ratio of 0.9, the radiated beam provides a gain of 21.4 dB at an angle of 19° while increasing f/D to 1.1 declined the gain slightly to 19.7 dB at 20°. Moreover, the side lobe levels in both cases are observed to be around 10 dB, which can potentially be caused by the tilt introduced in the planar reflector and may further be progressed by improving the phase distribution accurately.

9161, 2026, 1, Downloaded from https://onlinelibrary.wiley.com/doi/10.1155/js/8045999 by Muhammad Inam Abbasi - National Institutes Of Health Malaysia , Wiley Online Library on [11/01/2026]. See the Terms and Conditions (https://onlinelibrary.wiley.com/terms-and-conditions) on Wiley Online Library for rules of use; OA articles are governed by the applicable Creative Commons License

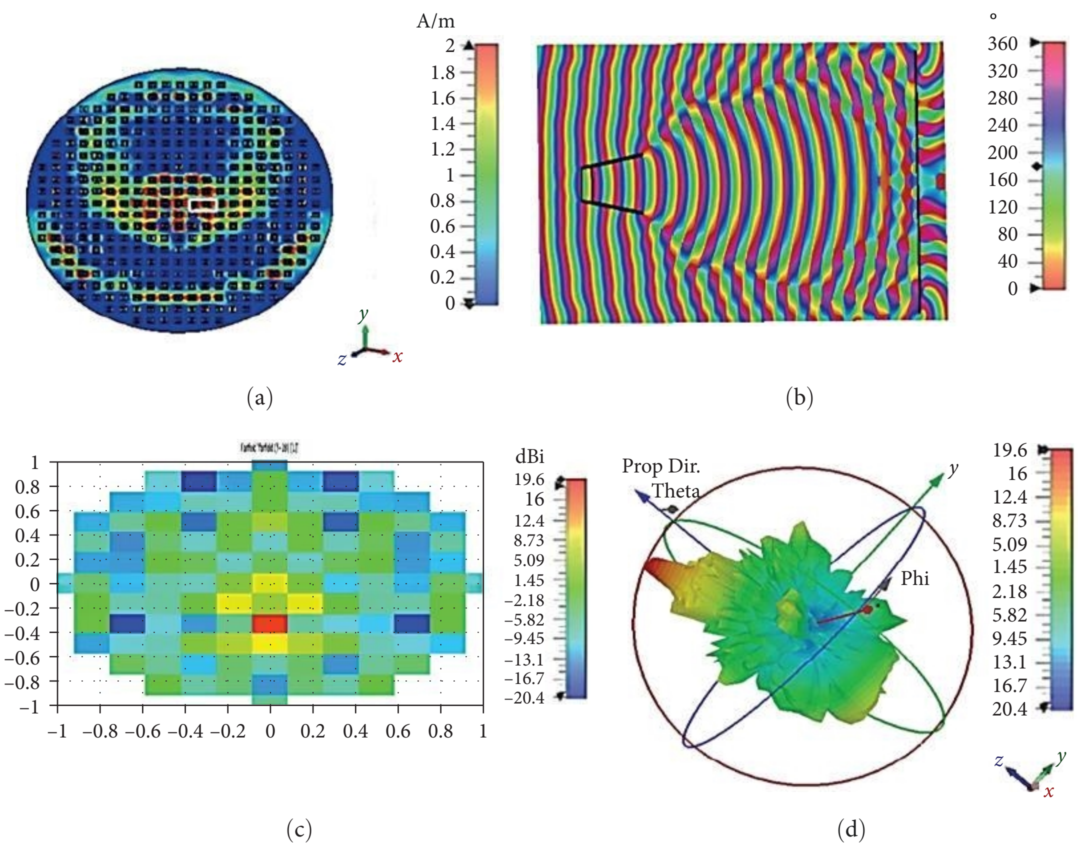

FIGURE 8: Electromagnetic analysis of a reflectarray antenna operating at 28 GHz with an *f*/*D* ratio of 1.1 (a) surface current distribution, (b) near-field phase distribution pattern, (c) 2D far-field radiation pattern, and (d) 3D far-field radiation pattern.

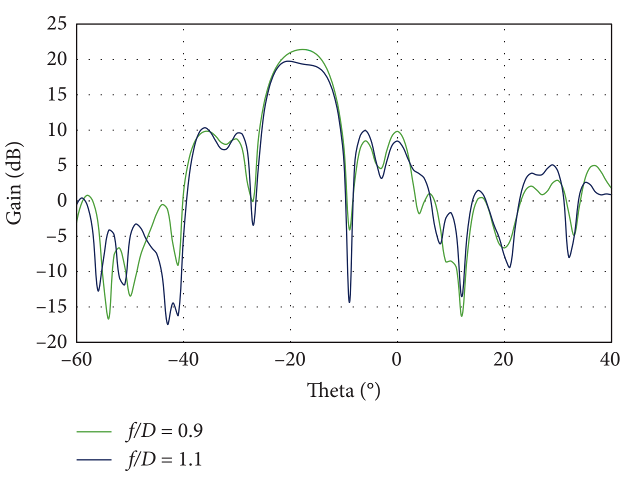

FIGURE 9: Far-field radiation patterns of a reflectarray antenna at 28 GHz for different *f*/*D* ratios.

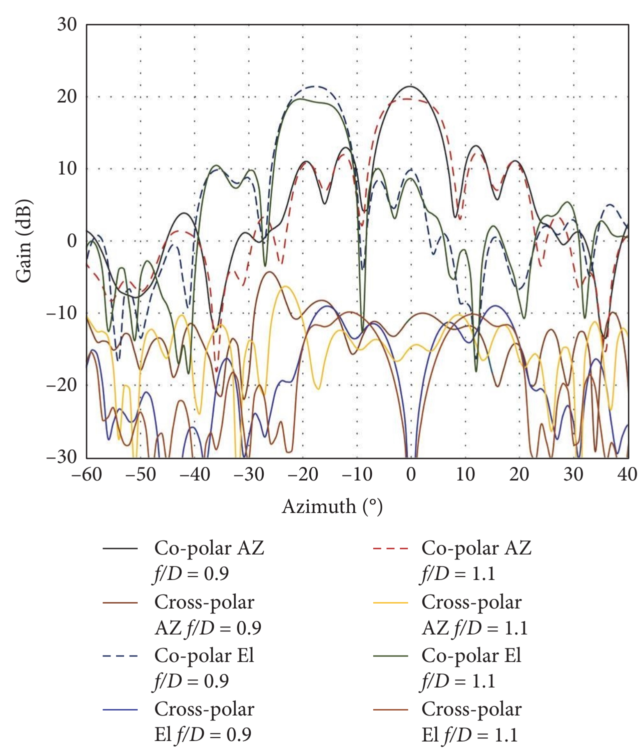

FIGURE 10: Radiation patterns for scanned beam reflectarray with cross-polar and co-polar components at 28 GHz.

Figure 10, shows the radiation patterns (co-polar and cross-polar) for a scanned beam RA at a given focal-to-diameter (*f*/*D*) ratio of 0.9 and 1.1. From the figure cross-polar remain below −25 dB in frequency range, suggesting good polarization purity and low interference from unwanted cross-polarization. This low level of cross-polar 25 indicates co-polar radiation is well-defined and strong, as the cross-polar remains suppressed across the angular range.

9161, 2026, 1, Downloaded from https://onlinelibrary.wiley.com/doi/10.1155/js/8045999 by Muhammad Inam Abbasi - National Institutes Of Health Malaysia , Wiley Online Library on [11/01/2026]. See the Terms and Conditions (https://onlinelibrary.wiley.com/terms-and-conditions) on Wiley Online Library for rules of use; OA articles are governed by the applicable Creative Commons License

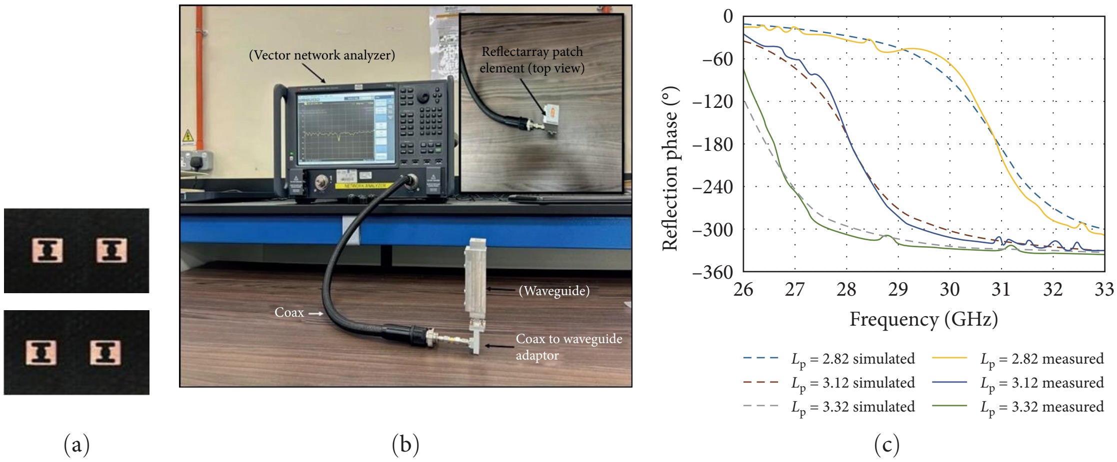

FIGURE 11: (a) Fabricated 2 patch element unit cells, (b) measurement setup, and (c) comparison of simulated and measured scattering parameters results.

5. Measurements and Comparison

The proposed unit cells were fabricated on Taconic TLY 3F substrate in order to verify the simulated results. Figure 11a shows the two element unit cells that have been fabricated for the verification of simulated results. 2×1 element RA unit cells were fabricated primarily to include the effect of mutual coupling during measurements. The measurement setup is also shown in Figure 11b, where a metallic waveguide was used for the scattering parameter measurements.

Figure 11c provides a comparison between the simulated and measured reflection phase results for different lengths of patch element unit cells. It can be observed from Figure 7 that the simulated and measured results demonstrate a very close agreement apart from some slight glitches in the measured results that are caused by the noise introduced by the measurement setup. Moreover, for all the patch lengths (L_p), the phase range is almost similar for simulations and measurements. The results verify the authenticity of the simulations and hence these elements have been considered suitable for the design of periodic array design.

Periodic RAs as explained in Section 3 were also fabricated. Figure 12a illustrates the fabricated prototypes of the proposed RA antenna, demonstrating a circular aperture carrying 357 unit cells. To facilitate experimental evaluation, the fabricated RA was mounted on a custom-designed 3D-printed acrylic stand, which was specifically engineered to allow fine adjustments of the f/D ratio and the overall tilt angle of the RA surface. Such mechanical flexibility ensured accurate alignment during measurements and enabled validation under conditions consistent with the proposed design specifications.

Far-field radiation measurements were performed to verify the simulated results using a compact antenna test range (CATR) facility, which provides a controlled environment for high-frequency antenna characterization. Figure 12b presents the measurement setup, where the RA antenna under test (AUT) was excited and its reflected signal was captured by a calibrated probe antenna positioned at the quiet zone of the CATR. A metallic reflective plate was strategically positioned within the measurement path to extend the effective separation between the AUT and the probe antenna, thereby ensuring compliance with the far-field criterion required for accurate pattern measurements. This arrangement effectively minimized near-field interactions and environmental scattering, enabling reliable validation of the simulated performance for both vertical and horizontal strip configurations.

Figure 12c demonstrates a comparison between simulated and measured radiation patterns of the proposed antenna. A close agreement between simulated and measured results can be observed in both cases where the maximum gain is observed to be around 21.4 dB with side lobes around 10 dB level. The main beam is also directed as per expectations to 19° while the cross-polar levels are at least 20 dB below the main beam.

Figure 13, illustrates the bandwidth performance of the designed RA antenna over 22–34 GHz for two focal-to-diameter ratios, $f/D = 0.9$ and $f/D = 1.1$. In terms of peak gain, the design achieves 21.4 dBi at $f/D = 0.9$ and 19.7 dBi at $f/D = 1.1$, maintaining relatively stable performance across the band. The 1-dB bandwidth is 16.9% at $f/D = 0.9\%$ and 23.21% at $f/D = 1.1$, indicating that the latter configuration provides a broader operational range and better frequency stability. Compared with previous studies, the proposed design provides 3.4/3.9 dB gain improvement with gains of about 20.7 dBi around 29 GHz.

Various RA antenna design presented in Table 2, demonstrated that the proposed design configurations, exhibits notable improvements in performance as compared to the previous studies. The design exhibits a gain of 21.4 dBi at $f/D = 0.9$ and 19.7 dBi at $f/D = 1.1$, as seen in Figure 12, surpassing [33], 3.4/3.9 dBi at 28/38 GHz and competing effectively with [30], 20.7 dBi at 29 GHz and [32], 20.2 dBi at 24 GHz. The 1-dB bandwidth is 16.9 % at $f/D = 0.9\%$ and 23.21% at $f/D = 1.1$, which, is higher than many other researches and remains appropriate for practical applications. This design's primary distinguishing characteristic is its capacity for a 19° beam scan, providing a notable

9161, 2026, 1, Downloaded from https://onlinelibrary.wiley.com/doi/10.1155/js/8045999 by Muhammad Inam Abbasi - National Institutes Of Health Malaysia , Wiley Online Library on [11/01/2026]. See the Terms and Conditions (https://onlinelibrary.wiley.com/terms-and-conditions) on Wiley Online Library for rules of use; OA articles are governed by the applicable Creative Commons License

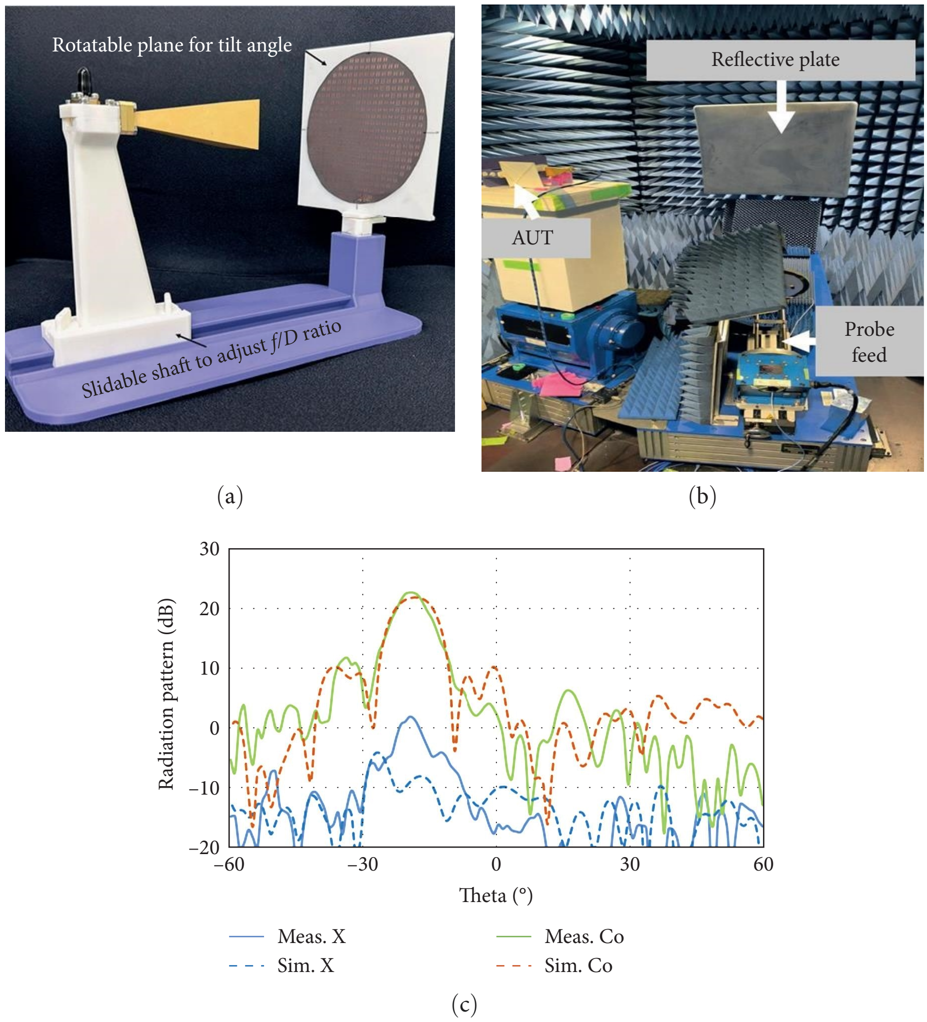

FIGURE 12: (a) Fabricated reflectarray antenna, (b) measurement setup for the reflectarray antenna in a compact chamber, and (c) comparison of simulated and measured results.

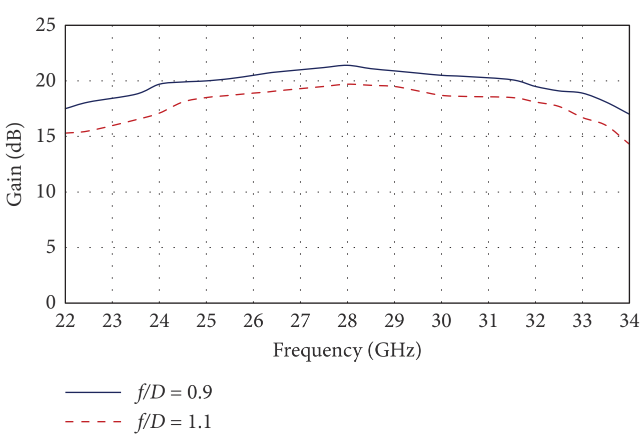

FIGURE 13: Bandwidth of designed RRA.

advantage over fixed-beam systems such as [30] and [31]. The results highlight the design's applicability for mm-wave applications, especially in 5G communications and satellite systems, where high gain, beam steering, and compact performance are essential. The suggested RA antenna constitutes a significant advancement in the area, harmonizing performance, functionality, and practicality.

6. Conclusion

The suggested RA antenna design, incorporating a rectangular patch with embedded slots forming an I-shape, exhibits notable improvements in bandwidth and performance. The investigation indicates that augmenting the f/D ratio from 0.9 to 1.1 enhances bandwidth from 16.9% to 23.21%, owing to improved phase distribution and diminished near-field effects. The novel I-shaped slot design enhances phase tuning, impedance matching, and aperture efficiency, while modifying surface current distribution for increased bandwidth and consistent gain. This concept surpasses traditional methods, rendering it a viable option for wideband applications like 5G and satellite systems, where high-frequency performance and adaptability are essential.

9161, 2026, 1, Downloaded from https://onlinelibrary.wiley.com/doi/10.1155/js/8045999 by Muhammad Inam Abbasi - National Institutes Of Health Malaysia , Wiley Online Library on [11/01/2026]. See the Terms and Conditions (https://onlinelibrary.wiley.com/terms-and-conditions) on Wiley Online Library for rules of use; OA articles are governed by the applicable Creative Commons License

Table 2: Performance comparison of the proposed technique with some relevant designs in literature.

Reference	Frequency (GHz)	Design shape	Design configuration	Gain (dB)	BW (%)	Array size
[30]	29	Meta surface	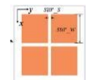	24	20.7	140 elements
[31]	26	Rec. patch/cir. patch	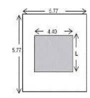	25.2/ 26.45	13.6/ 13.1	20 × 20
[32]	24	Circular ring	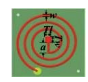	20.2	16.7	10 × 10
[33]	28/38	H shaped		21/25	3.4/3.9	3 × 11
[34]	26	Circular ring	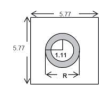	26.47	13.1	20 × 20
This work	28	Rect. patch with I-shaped slot		21.4	16.9/ 23.21	357 elements

Data Availability Statement

The data that support the findings of this study are available from the corresponding author upon reasonable request.

Disclosure

All the authors have reviewed the final manuscript and agree to be accountable for all aspects of the work presented.

Conflicts of Interest

The authors declare no conflicts of interest.

Author Contributions

S. D. Khan contributed to conceptualization, software, measurements, and preparation of the original draft. M. I. Abbasi contributed to supervision, project administration, funding, data collection, software, measurements, and preparation of the original draft. I. M. Ibrahim contributed to supervision, project administration, and reviewing of the original draft. N. H. Sulaiman was responsible for visualization, methodology design, and reviewing of the original draft. M. H. Dahri contributed to resources, methdology, and conceptualization. M. A. Humayun was responsible for project administration, software, and preparation of the original draft. Hela Elmannai contributed to software, funding, and data collection.

Funding

The study was funded by the Ministry of Higher Education (MOHE) of Malaysia through the Fundamental Research Grant Scheme (FRGS) (Grant FRGS/1/2023/TK07/UTEM/02/7). Princess Nourah bint Abdulrahman University Researchers Supporting Project Number (PNURSP2026R747), Princess Nourah Bint Abdulrahman University, Riyadh, Saudi Arabia.

Acknowledgments

The author would like to thank the staff of UTeM for technical support.

References

[1] J. Huang and J. A. Encinar, *Reflectarray Antennas* (John Wiley & Sons, 2008).

[2] A. Ahmed Mugheri, M. I. Abbasi, I. Mohd Ibrahim, et al., "Recent Advances in Transparent Reflectarray Antennas," *IEEE Access* 13 (2025): 161541–161572.

[3] P. Zhang, X. Zhu, X. Shu, C. Zhao, Z. Tao, and P. Chu, "A 20/30GHz Dualband Dual Circularly Polarized Antenna Hybridizing Folded Refelctarray and Folded Transmitarray," in *2022 IEEE MTT-S International Wireless Symposium (IWS)*, (Harbin, China: IEEE, 2022), 1–3.

[4] P. Zhang, X. Zhu, X. Shu, C. Zhao, Z. Tao, and P. Chu, "2022 IEEE MTT-S International Wireless Symposium (IWS)," in *A 20/30GHz Dualband Dual Circularly Polarized Antenna Hybridizing Folded Refelctarray and Folded Transmitarray*, (Harbin, China: IEEE, 2022), 1–3.

[5] X. Yang, S. Xu, F. Yang, et al., "A Broadband High-Efficiency Reconfigurable Reflectarray Antenna Using Mechanically Rotational Elements," *IEEE Transactions on Antennas and Propagation* 65, no. 8 (2017): 3959–3966.

[6] P. Mei, S. Zhang, and G. F. Pedersen, "A Low-Cost, High-Efficiency and Full-Metal Reflectarray Antenna with Mechanically 2-D Beam-Steerable Capabilities for 5G Applications," *IEEE Transactions on Antennas and Propagation* 68, no. 10 (2020): 6997–7006.

[7] M. H. Dahri, M. H. Jamaluddin, F. C. Seman, et al., "Aspects of Efficiency Enhancement in Reflectarrays With Analytical

9161, 2026, 1, Downloaded from https://onlinelibrary.wiley.com/doi/10.1155/js/8045999 by Muhammad Inam Abbasi - National Institutes Of Health Malaysia , Wiley Online Library on [11/01/2026]. See the Terms and Conditions (https://onlinelibrary.wiley.com/terms-and-conditions) on Wiley Online Library for rules of use; OA articles are governed by the applicable Creative Commons License

Investigation and Accurate Measurement," *Electronics* 9, no. 11 (2020): 1887.

[8] Z. Y. Yu, Y. H. Zhang, S. Y. He, H. T. Gao, H. T. Chen, and G. Q. Zhu, "A Wide-Angle Coverage and Low Scan Loss Beam Steering Circularly Polarized Folded Reflectarray Antenna for Millimeter-Wave Applications," *IEEE Transactions on Antennas and Propagation* 70, no. 4 (2022): 2656–2667.

[9] M. Inam, M. H. Dahri, M. R. Kamarudin, et al., "Linearly Polarized Millimeter Wave Reflectarray With Mutual Coupling Optimization," *Computers, Materials and Continua* 72, no. 2 (2022): 2397–2410.

[10] D. Berry, R. Malech, and W. Kennedy, "The Reflectarray Antenna," *IEEE Transactions on Antennas and Propagation* 11, no. 6 (1963): 645–651.

[11] J. Tang, S. Xu, F. Yang, and M. Li, "Design and Measurement of a Reconfigurable Transmitarray Antenna With Compact Varactor-Based Phase Shifters," *IEEE Antennas and Wireless Propagation Letters* 20, no. 10 (2021): 1998–2002.

[12] W. Li, H. Tu, Y. He, L. Zhang, S.-W. Wong, and S. Gao, "A Novel Wideband Tightly Coupled Dual-Polarized Reflectarray Antenna," *IEEE Transactions on Antennas and Propagation* 71, no. 6 (2023): 5422–5427.

[13] M. I. Abbasi and M. Y. Ismail, "Reflection Loss and Bandwidth Performance of X-Band Infinite Reflectarrays: Simulations and Measurements," *Microwave and Optical Technology Letters* 53, no. 1 (2011): 77–80.

[14] M. Y. Ismail and M. Inam, "Resonant Elements for Tunable Reflectarray Antenna Design," *International Journal of Antennas and Propagation* 2012, no. 1 (2012): 914868.

[15] J. Qin, M. Sun, and A. Chen, "A Synthesis Approach for Enhancing the Aperture Efficiency of Wideband Reflectarray Antennas," *IEEE Antennas and Wireless Propagation Letters* 23, no. 12 (2024): 4817–4821.

[16] H. Zhang, Y. Wang, J. Wang, H. Xiao, X. Chen, and X. Wang, "A Single-Layer Circularly Polarized Reflectarray Antenna With High Aperture Efficiency for Microwave Power Transmission," *International Journal of Antennas and Propagation* 2023, no. 1 (2023): 1569710.

[17] J. Shi, J. Zhou, L. Cai, Z. H. Jiang, and W. Hong, "A High-Efficiency Single-Layer Broadband Reflectarray Antenna for 60 GHz Applications," *IEEE Antennas and Wireless Propagation Letters* 24, no. 8 (2025): 2557–2561.

[18] Z. X. Wang, H. Q. Yang, F. Zhai, J. W. Wu, Q. Cheng, and T. J. Cui, "A Low-Cost and Low-Profile Electronically Programmable Bit Array Antenna for Two-Dimensional Wide-Angle Beam Steering," *IEEE Transactions on Antennas and Propagation* 71, no. 1 (2023): 342–352.

[19] Y. Wang, S. Xu, F. Yang, and M. Li, "A Novel 1-Bit Wide-Angle Beam Scanning Reconfigurable Transmitarray Antenna Using an Equivalent Magnetic Dipole Element," *IEEE Transactions on Antennas and Propagation* 68, no. 7 (2020): 5691–5695.

[20] W. Li, T. Qiu, J. Wang, et al., "Programmable Coding Metasurface Reflector for Reconfigurable Multibeam Antenna Application," *IEEE Transactions on Antennas and Propagation* 69, no. 1 (2021): 296–301.

[21] X. Zong, F. Yang, S. Xu, and M. Li, "A Study of Spatial Quantization Effects on Reconfigurable Reflectarray Antennas," *IEEE Antennas and Wireless Propagation Letters* 24, no. 8 (2025): 2607–2611.

[22] C. W. Luo, G. Zhao, Y. C. Jiao, G. T. Chen, and Y. D. Yan, "Wideband 1-Bit Reconfigurable Transmitarray Antenna Based on Polarization Rotation Element," *IEEE Antennas and Wireless Propagation Letters* 20, no. 5 (2021): 798–802.

[23] N. Zhang, K. Chen, J. Zhao, et al., "A Dual-Polarized Reconfigurable Reflectarray Antenna Based on Dual-Channel Programmable Metasurface," *IEEE Transactions on Antennas and Propagation* 70, no. 9 (2022): 7403–7412.

[24] H. Huang, J. Ye, C. Xue, and T. Li, "Circular Polarization Selective Metasurface for Folded Reflectarray Antenna at Ka Band," *IEEE Antennas and Wireless Propagation Letters* 24, no. 5 (2025): 1278–1282.

[25] N. Qin and L. Guo, "On the Use of Metallic Polarization Conversion Element With Continuous 360° Phase for High-Efficiency All-Metal Planar Folded Reflectarrays," *IEEE Antennas and Wireless Propagation Letters* 23, no. 6 (2024): 1859–1863.

[26] P.-P. Zhang, X.-C. Zhu, S.-Y. Qian, L. Cheng, and G.-Y. Tu, "A Bandwidth-Enhanced Circularly Polarized Reflectarray Antenna With Ultralow-Profile Pancharatnam–Berry Metasurface," *IEEE Antennas and Wireless Propagation Letters* 23, no. 12 (2024): 4129–4133.

[27] Z. H. Jiang, Y. Zhang, and W. Hong, "Anisotropic Impedance Surface Enabled Low-Profile Broadband Dual-Circularly Polarized Multibeam Reflectarrays for Ka-Band Applications," *IEEE Transactions on Antennas and Propagation* 68, no. 8 (2020): 6441–6446.

[28] R. Shamsaee Malfajani, K. Glatre, and J.-J. Laurin, "Wideband True-Time-Delay Dual-Polarized Reflectarray Antenna for Satellite Applications," *IEEE Transactions on Antennas and Propagation* 73, no. 7 (2025): 4336–4348.

[29] Y. Cao, W. Che, W. Yang, C. Fan, and Q. Xue, "Novel Wideband Polarization Rotating Metasurface Element and Its Application for Wideband Folded Reflectarray," *IEEE Transactions on Antennas and Propagation* 68, no. 3 (2020): 2118–2127.

[30] M. Guo, L. Guo, W. Feng, and X. Chen, "A Single-Layered Broadband Reflectarray Employing 0.15-Wavelength Elements," *IEEE Antennas and Wireless Propagation Letters* 22, no. 2 (2023): 318–322.

[31] Y. Li, M. E. Bialkowski, K. H. Sayidmarie, and N. V. Shuley, "81-Element Single-Layer Reflectarray With Double-Ring Phasing Elements for Wideband Applications," in *IEEE Antennas and Propagation Society International Symposium, 2010* (2010): 1–4.

[32] L. Guo, P. K. Tan, and T. H. Chio, "Single-Layered Broadband Dual-Band Reflectarray With Linear Orthogonal Polarizations," *IEEE Transactions on Antennas and Propagation* 64, no. 9 (2016): 4064–4068.

[33] X. Li, Y. Wan, J. Liu, et al., "Broadband Electronically Scanned Reflectarray Antenna With Liquid Crystals," *IEEE Antennas and Wireless Propagation Letters* 20, no. 3 (2021): 396–400.

[34] S. Costanzo, F. Venneri, A. Borgia, and G. Di Massa, "A Single-Layer Dual-Band Reflectarray Cell for 5G Communication Systems," *International Journal of Antennas and Propagation* 2019 (2019): 9479010.

[35] M. I. Abbasi, M. H. Dahri, M. H. Jamaluddin, N. Seman, M. R. Kamarudin, and N. H. Sulaiman, "Millimeter Wave Beam Steering Reflectarray Antenna Based on Mechanical Rotation of Array," *IEEE Access* 7 (2019): 145685–145691.

9161, 2026, 1, Downloaded from https://onlinelibrary.wiley.com/doi/10.1155/js/8045999 by Muhammad Inam Abbasi - National Institutes Of Health Malaysia , Wiley Online Library on [11/01/2026]. See the Terms and Conditions (https://onlinelibrary.wiley.com/terms-and-conditions) on Wiley Online Library for rules of use; OA articles are governed by the applicable Creative Commons License